Polymer 168 (2019) 131–137

Contents lists available at ScienceDirect

Polymer

journal homepage: www.elsevier.com/locate/polymer

Amino graphene oxide/dopamine modified aramid fibers: Preparation, epoxy nanocomposites and property analysis

Xianyun Gong[a], Yuyan Liu[b,*], Youshan Wang[c], Zhimin Xie[c], Qingliang Dong[b], Mengyao Dong[d,e], Hu Liu[e], Qian Shao[f], Na Lu[g], Vignesh Murugadoss[d], Tao Ding[h,**], Zhanhu Guo[d,***]

[a] School of Food Engineering, Department of Chemistry, Harbin University, Harbin 150086, China
[b] MIIT Key Laboratory of Critical Materials Technology for New Energy Conversion and Storage, School of Chemistry and Chemical Engineering, Harbin Institute of Technology, Harbin 150001, China
[c] National Key Laboratory of Science and Technology on Advanced Composites in Special Environment Center for Composite Materials and Structures, Harbin Institute of Technology, Harbin 150001, China
[d] Integrated Composites Laboratory (ICL), Department of Chemical & Biomolecular Engineering, University of Tennessee, Knoxville, TN 37996, USA
[e] Key Laboratory of Materials Processing and Mold (Zhengzhou University), Ministry of Education; National Engineering Research Center for Advanced Polymer Processing Technology, Zhengzhou University, Zhengzhou, 450002, Henan, China
[f] School of Materials Science and Engineering, Shandong University of Science and Technology, Qingdao 266590, China
[g] Lyles School of Civil Engineering, School of Materials Engineering, Birck Nanotechnology Center, Purdue University, West Lafayette, IN 47906, USA
[h] College of Chemistry and Chemical Engineering, Henan University, Kaifeng 475004, China

HIGHLIGHTS

- The self-polymerized polydopamine) (PDA) layer was deposited on aramid fibers.
- An efficient route to functionalize aramid fibers based on dopamine chemistry was developed.
- With PDA coating and further amino GO grafting, the rougher fiber surface significantly improved the IFSS.

ARTICLE INFO

Keywords:
Polydopamine
Amino graphene oxide
Interface properties

ABSTRACT

Dopamine modified aramid fiber (AF) surface was grafted with amino functionalized graphene oxide to improve the interfacial adhesive performance. The self-polymerized polydopamine (PDA) coating and subsequent amino GO grafting on the AF surface attributed to the increase in its surface roughness and surface-active groups. The functional groups, chemical composition and surface topography of unmodified and modified AF was investigated by Fourier transform infrared (FTIR) spectroscopy, X-ray photoelectron spectroscopy (XPS) and Scanning electron microscopy (SEM). The interfacial properties were analyzed by measuring interfacial shear strength (IFSS) of unmodified and modified AF embedded epoxy matrix. Further, the properties were tuned by optimizing the reaction temperature and concentration of ethylenediamine. The IFSS of AF/epoxy composites was increased by 34% after grafting amino graphene oxide.

1. Introduction

With unique properties such as high strength (the single filament strength of aramid fiber can reach 3850 MPa), good toughness (the impact strength is 6 times that of graphite fibers), low weight (the density of AF is 1.44 g/cm^3), low dielectric constant (the dielectric constant of aramid fiber which contained 58% fibers in the epoxy composites is 3.3), and good thermal resistance (the thermal decomposition temperature is over 550 °C), aramid fibers (AF) have been a potential reinforcement material for multi-functional composites used in automobile, aviation, space, bullets, protective garments, electromagnetic interference shielding, etc [1–7]. However, their poor interfacial adhesion with the matrix due to the smooth surface and chemical inertness limits their applications in the composite materials. Therefore,

* Corresponding author.
** Corresponding author.
*** Corresponding author.
E-mail addresses: liuyy@hit.edu.cn (Y. Liu), dingtao@henu.edu.cn (T. Ding), zguo10@utk.edu (Z. Guo).

https://doi.org/10.1016/j.polymer.2019.02.021
Received 22 November 2018; Received in revised form 2 February 2019; Accepted 10 February 2019
Available online 12 February 2019
0032-3861/

many research efforts have been made to improve the interfacial properties of AF based composites through the modification of AF surface by plasma treatment, chemical etching, ion sputtering, ultrasonic treatment, corona discharge and so on [8–10]. Unfortunately, these techniques have drawbacks such as multi-step procedures, high cost, toxic by-products, deterioration of the structure and the properties of fibers, thereby restricting the potential performance of the composites [11]. Furthermore, it is worth pointing out that the fiber coating or sizing during composite processing prevents it from breaking and fluffing compared to chemical treatment [12,13].

Very recently, the treatment of fibers using dopamine has attracted research interests due to the advantages such as remarkable chemical properties, mild reaction conditions, low cost, and easy applicability to different materials including non-stick surfaces of various size and shape [14]. Usually, the catechol groups in the dopamine undergo self-oxidative polymerization under the weak alkaline condition to form polydopamine coating on the fibers [15]. Yang et al. demonstrated that the functionalization of graphene with PDA improved their dispersibility and stress transfer between the polyurethane and the graphene [16]. In our earlier work, we modified the surface of AF using dopamine and investigated the effect of treatment time and dopamine concentration. It was found that the AF modified with PDA exhibited an improved interfacial shear strength (IFSS). Moreover, the catechol groups reacted with thiol- or amine-functional groups through Schiff base reactions or Michael addition under oxidizing conditions [17,18]. This facilitated the grafting of functionalized secondary materials onto PDA, which further improved their functionality and surface reactivity [16,19]. Zhu et al. found that the grafting of graphene oxide on PDA coated aramid fibers increases their mechanical properties as well as UV-resistance [20]. Sa et al. reported that grafting of epoxy functionalized silane improved the adhesion strength of PDA functionalized meta-aramid fibers in rubber matrix by 62.5% [21]. In view of these, it is valid to expect the grafting of amino-functionalized graphene oxide on PDA coated aramid fibers to be effective for improving their adhesive performance in an epoxy matrix. Herein, amino graphene oxide was grafted onto the surface of aramid fibers/modified polydopamine-capped utilizing the secondary reaction of active hydrogen in polydopamine. The physical properties of the pure AF and modified AF were investigated by (FT-IT) spectroscopy, scanning electron microscopy (SEM) and X-ray photoelectron spectroscopy (XPS). The interfacial adhesive performance of modified AF was analyzed by measuring the IFSS. It is found that the properties of the PDA modified AF varies with varying the reaction temperature and concentration of ethylenediamine during grafting of amino graphene oxide.

2. Experimental

2.1. Materials

3,4-dihydroxyphenethylamine hydrochloride (DOPA, 98%), and tris (hydroxymethyl)aminomethane (TRIS, 99%) were purchased from J&K Chemicals Ltd. Ethylenediamine (EDA) and graphite powders were obtained from Aladdin Reagent Corp. (Shanghai, China). KEVLAR49 was obtained from J&K Chemicals (DuPont Company, America). The matrix, epoxy resin (E51) and curing agent, m-Xylylenediamine were procured from Shanghai Resin, China. All the chemical reagents and solvents were of analytical grade and used as received without any further treatment.

2.2. Preparation of amino graphene oxide sample

The graphene oxide (GO) nanosheets were prepared by the modified Hummer's method [22]. Briefly, 0.1 g GO was dispersed into 100 mL deionized water via ultrasonication for 15 min, configured as 1 g/L GO solution. Then, a certain amount of EDA was added to the GO solution at 60 °C and later on stirred for 12 h. The solid products were collected by washing with a copious amount of deionized water and subsequently dried at 40 °C under vacuum.

2.3. Preparation of amino GO/dopamine modified aramid fibers

Firstly, the as-received AF were extracted with acetone for 24 h to eliminate the commercial sizing and subsequently dried at 40 °C for 6 h under vacuum. To functionalize the surface of AF, the 2 mm long desized-AF were immersed in a buffer solution (pH = 8.5), and then dopamine was added. The above mixture was sonicated for 10 min and kept under constant stirring for 24 h at room temperature. PDA coating was formed on the desized-AF surface by self-oxidative polymerization of dopamine. The PDA-coated AF was washed and filtered with deionized water to remove residual dopamine and PDA. The filtrate was then dried at 40 °C for 5 h in vacuum. To obtain amino GO/dopamine modified aramid fibers, PDA-aramid fibers were added into amino GO solution to react through amine-catechol adduct formation at 15–50 °C for 12–24 h, the amino GO-grafted dopamine modified aramid fibers were obtained and dried at 50 °C for 24 h under a vacuum.

The mixture of epoxy resin E−51 and m-xylylenediamine in the weight ratio of 100:18.32 was applied on a single aramid fiber to form resin microdroplet. The resin microdroplet was then cured at 60 °C for 1 h and at 100 °C for 2 h. The prepared resin microdroplets were used to test the interfacial properties of the modified fibers.

2.4. Characterizations

The molecular elucidation of the GO, amino GO, pure AF and surface modified AF was carried out by Fourier transform infrared (FTIR) spectroscopy (Nicolet spectrometer) in the wavenumber range between 400 and 4000 cm^{-1} at a resolution of 4 cm^{-1}. The morphologies of GO and amino GO were investigated using transmission electron microscopy (Libra 120). The functional groups and chemical composition of the amino GO and surface modified AF surface were characterized by X-ray photoelectron spectroscopy (ESCALAB 220i-XL) with Al-Kα radiation. The signals were collected at the 45° of incidence angle. The surface topography of the pure AF, PDA-AF and amino GO/PDA-AF was observed by using a scanning electron microscope (SEM, Quanta 200 FEG).

The micro-debonding test for the prepared resin droplets was carried out on an XQ-1 fiber tensile testing machine to investigate the interfacial properties at a displacement rate of 0.1 mm/min. The IFSS (τ) was calculated using Equation (1) [23]:

$$\tau = F_{max}/(\pi D_f L_e) \quad (1)$$

where F_{max} is maximum pullout force, D_f is the diameter of AF, and L_e is the length of AF embedded in the epoxy matrix. The experiment was repeated for 30 times and the average value was calculated for each sample.

3. Results and discussion

3.1. Characterization of GO and amino GO

The preparation process of the Amino GO-PDA-AF/EP is illustrated in Scheme 1. At first, the PDA was attached to the surface of AF via the strong adhesion of dopamine. This is because the PDA was coated on the AF surface through an intermolecular cross-linking of 5, 6-dihydroxyindole resulted from the oxidative conversion of the catechol groups in dopamine under basic conditions [24–26]. Moreover, this reaction introduced polar hydroxyl and imine groups to the PDA. Subsequently, the Michael addition reaction between amines and oxidized quinone structures resulted in the grafting of amino GO on PDA-AF, which was beneficial to improve the surface activity of the fiber and its interfacial bonding with the epoxy resin.

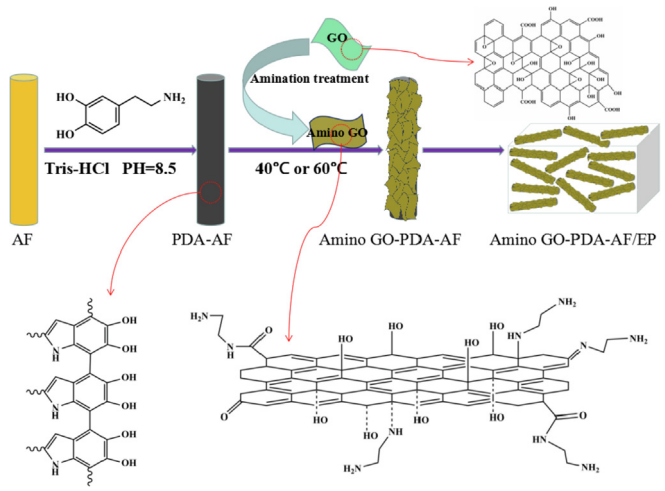

Scheme 1. Illustration of the manufacturing process of Amino GO-PDA-AF/EP.

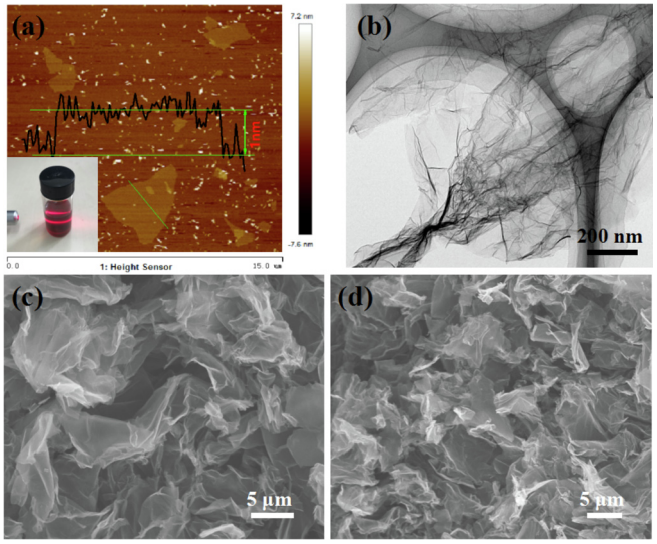

Fig. 1. (a) AFM image of GO and the digital photograph of GO solution is shown in the inset. (b) TEM image of GO. SEM images of (c) GO and (d) amino GO.

The morphologies of the as-obtained graphene oxide (GO) and amino GO are shown in Fig. 1. The cross-sectional view of the atomic force microscopy (AFM) image demonstrates that the average thickness of GO is about 1 nm, and a large lateral size exceeds several micrometer (Fig. 1a). It is important to note that a Tyndall effect can be clearly observed in the inset of Fig. 1a, indicating its superior dispersity and hydrophilicity. A typical TEM image of GO reveals a thin gauze and wrinkled morphology (Fig. 1b), demonstrating its excellent flexibility and machinability. In addition, the SEM image of GO also shows similar results to its TEM (Fig. 1c). Interestingly, the morphology of amino GO is basically the same as that of GO, indicating that the amination modification had little effect on the morphology of GO.

The FTIR spectra of GO and amino GO are shown in Fig. 2. It can be seen that the amino GO exhibits the variation in the range between 1465 and 1255 cm^{-1} that is ascribed to the stretching of C—N and bending of NH_2 and —NH— groups. In addition, the observed widening of the peak at 3430 cm^{-1} represents the combination of O—H and N—H stretching.

Raman spectra of graphite, GO, and amino GO with their characteristic G- and D-bands are shown in Fig. 3. The characteristics G band representing the in-plane vibration of sp^2 bonded carbon atoms is observed for graphite [27–29]. The intensity of the D band associated

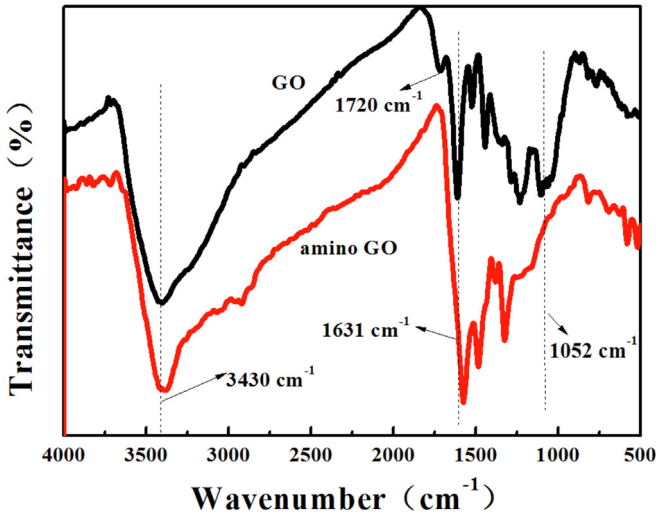

Fig. 2. FTIR spectra of graphene, GO and amino GO, respectively.

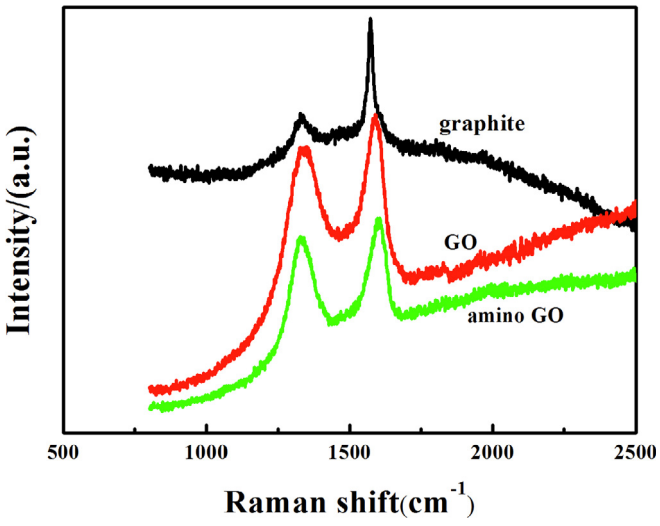

Fig. 3. Raman spectra of graphene GO and amino GO, respectively.

with the crystalline grain size and impurity defects of graphite is insignificant because of its crystal symmetries [30]. Interestingly, the GO and amino GO exhibit strong G and D bands. This can be explained through the following reasons. The chemical method adopted for the preparation of GO involved the exfoliation and introduction of oxygen within the graphite layers, which increased the defects of crystals and reduced the number of layers [31,32]. The GO was then reduced with EDA to produce amino GO; however, the reduction reaction caused the fracture of carbon bond and made the crystal sizes smaller [33].

FTIR spectra of amino GO obtained at different temperatures are shown in Fig. 4a. It depicts that the representative peaks of amino GO between 1465 and 1255 cm^{-1} and at around 3430 cm^{-1} (ref. Fig. 2) become intense and wider with the increase in the preparation temperature. These results indicate that the amount of amino-functional group grafted on GO increases with increasing the temperature. Further, the disappearance of the peaks at 1713 and 1070 cm^{-1} corresponding to C=O and C—O, respectively, indicates that the degree of reduction of GO was increased gradually with increasing temperature [34]. Also, the intensity of their characteristic peaks increases with increasing the concentration of EDA as seen in Fig. 4b, which indicates that increasing the concentration of EDA was helpful to improve the functionalization in GO.

The results of the GO XPS spectrum show that the pristine GO was

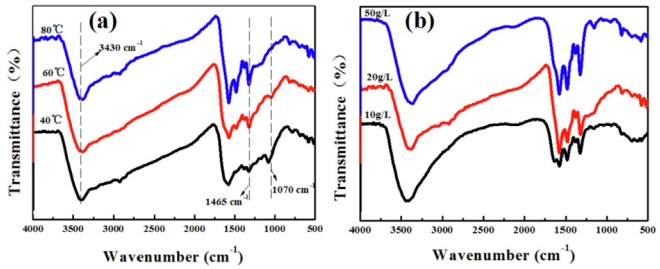

Fig. 4. FTIR spectra of (a) amino GO at different preparation temperatures and (b) amino GO at different preparation concentrations of EDA.

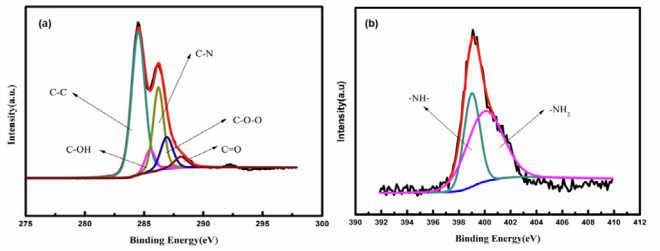

Fig. 5. (a) C1s and (b) N1s XPS spectra of amino GO.

Table 1
Structure and compositions analysis of C1s Peaks of amino GO.

Chemical bond	Peak position	Peak area	Content (%)
C—C	284.5	63402.77	53.88
C—O	285.5	7586.01	6.45
C—N	286.2	28819.44	24.49
C—O—C	286.9	12972.63	11.02
C=O	288.1	4894.75	4.16

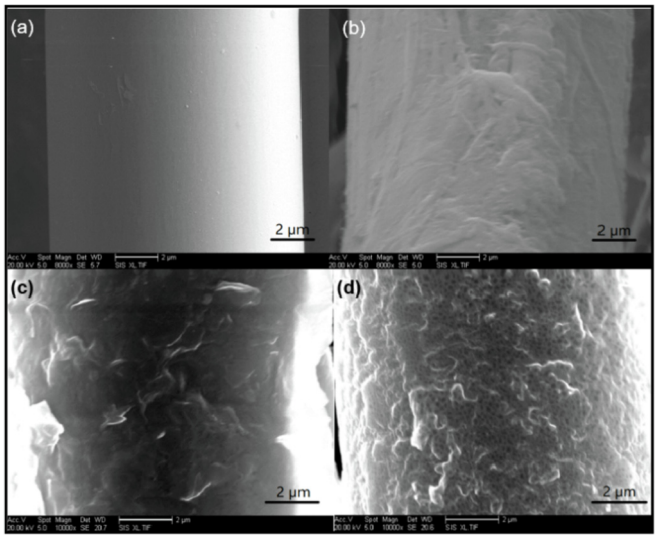

Fig. 6. SEM images of the surfaces of **(a)** pure desized-AF, **(b)** PDA-AF, **(c)** amino GO-PDA-AF prepared at 40 ℃, and **(d)** amino GO-PDA-AFs prepared at 60 ℃.

comprised of carbon (C) and oxygen (O) species with the oxygen to carbon signal ratio (O/C) of 0.683. This means that the graphene was well oxidized. However, the results of the amino GO XPS spectrum in Fig. 5 show that the amino GO was composed of carbon (C), oxygen (O) and nitrogen (N) elements. Compared with GO, N element content increased from 0 to 7.02%. In addition, the O element content decreased from 40.58% to 24.98%, which indicated that EDA had a certain

Table 2
Structure and compositions analysis of C1s Peaks of amino GO/dopamine modified aramid fibers.

Chemical bond	Peak position	Peak area	Content (%)
C—C	284.6	28070.87	45.00
C—O	285.6	8312.58	13.33
C—N	286.2	13490.92	21.63
C—O—C	286.9	5520.67	8.85
C=O	288.1	6975.14	11.18

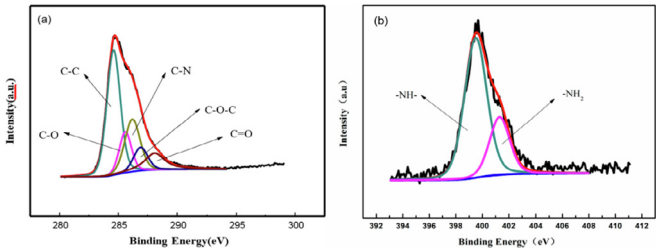

Fig. 7. (a) C1s and **(b)** N1s XPS spectra of amino GO/dopamine modified aramid fibers.

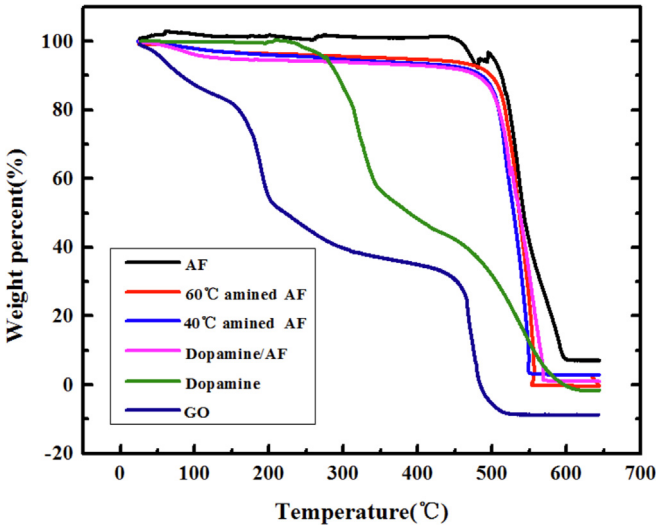

Fig. 8. TGA curves of AF, amined AF, Dopamine/AF and GO.

reduction effect on the GO. The C1s spectra of amino GO were deconvoluted into five peaks corresponding to C—C at 284.5 eV, C—O at 285.5 eV, C—N at 286.2 eV, C—O—C at 286.9 eV, and C═O at 288.1 eV [35]. The results are summarized in Table 1. Compared with the C1s spectra of GO, a C—N peak appeared, the content was 24.49%. The C—O—C peak became smaller significantly, the content decreased from 42.35% to 11.02%. The content of C—O and C═O also slightly declined. These indicate the chemical reaction between EDA and GO. Meanwhile, at the time of reaction, the O atoms, which contained in the C—O—C, disappeared. In addition, the content of C—C increased from 34.71% to 53.88% compared with GO, indicating that EDA repaired the damaged C—C sp^2 hybrid structure and reduced the GO indeed to some extent.

The N_{1s} spectra of amino GO were fitted into two peaks at 399 and 400.5 eV attributed to the —NH— and —NH_2— groups, respectively [36]. The —NH— was distributed at one end of the combination of EDA and GO, while the NH_2 was at the other end of the EDA. It can be clearly seen from the diagram that the —NH-peak area was obviously larger than that of the —NH_2 peak area. This was because that a part of EDA was connected between two GO layers, making the content of —NH— more than that of the —NH_2—. However, due to excess EDA, there was a considerable portion of the —NH_2 available, these —NH_2 group

Table 3
IFSS test results of AF/epoxy composites modified at different condition.

Content	unmodified	dopamine modified	amino GO/dopamine modified at 40 °C	amino GO/dopamine modified at 60 °C
IFSS(MPa)	26.31 ± 1.3	34.73 ± 2.2	31.52 ± 1.6	35.21 ± 0.9

provided the active sites of the reaction when the amino GO was grafted to the AF for the next step.

3.2. Research on amino GO/dopamine modified aramid fibers

SEM images depicting the surface morphology of pure desized-AF, PDA-AF and amino GO/PDA-AF prepared at different reaction temperatures are shown in Fig. 6. It can be observed that the pure AF possess clean and smooth surface, and contain some shallow and narrow micro-grooves along the axial direction (Fig. 6a). After treatment with dopamine, the PDA-AF displayed a high roughness surface with significant protuberances, indicating the coating of dopamine on the AF surface by self-oxidative polymerization (Fig. 6b). Fig. 6c and d shows that the amino GO/PDA-AF are covered with flakes of amino GO. It can be clearly seen that the obtained surface of amino GO/PDA-AF becomes more uneven and much rougher, which is beneficial to improve the surface activity of the fiber and its interfacial bonding with the resini. Moreover, it was also observed that the surface roughness of PDA-AF and the density of amino GO on their surface increased with the increase of the reaction temperature from 40 to 60 °C, and the results are consistent with those of the FTIR spectrum analysis. All above results indicate that AF were successfully modified by dopamine treatment and further grafted with amino GO by reaction with EDA, which gave them the potential to strengthen the epoxy resins.

The surface chemical compositions of amino GO/dopamine modified aramid fibers were further analyzed by using XPS. The results are presented in Table 2. It can be seen that after grafting, N element content of the modified fibers surface was 9.6%, which was greater than that of the amino GO and less than PDA. The content of C element was 68.56%, more than 67.37% of PDA. In addition, the content of O element was 21.84%, less than the content of O in PDA. All these indicate that the amino GO had been grafted on the AF.

For amino GO/dopamine modified aramid fibers, the C1s spectra were fitted into five peaks at 284.6 (C—C), 285.6 (C—O), 286.2 (C—N), 286.9 (C—O), and 288.1 eV (C═O), respectively (Fig. 7a), consistent with the previous report [37]. Compared with the C1s spectra of amino GO, the C—C and C—N bond contents decreased, however, C—O and C—N contents increased, all functional group ratios were close to the value of pure PDA. The results indicated that the grafting process incorporated the nitrogen atoms into the AF surfaces. The amino GO had been successfully grafted on the AF, but it had not completely covered the AF, or the thickness was less than the detection depth of XPS. Fig. 7b shows that the N1s spectra of amino GO/dopamine modified AF can be fitted into only two peaks with BEs at about 399.5 (−NH) and 401.4 eV (NH_2) [38]. Compared with the N1s fitted results of PDA- AF, the = N—H peak in PDA coating disappeared, and the intensity of the $-NH_2$ peak in the amino GO increased. This indicated that the amino GO had completely covered the AF, but the thickness of the amino GO coating has not yet exceeded the detection depth of XPS. The exact contents of PDA coating on AF and amino GO on the surface modified AF can be determined by using thermogravimetric analysis (TGA). As known from the calculation (Fig. 8), the content of the PDA coating on AF is 9.2%, and the amino GO on the AF surface modified at temperature of 40 °C and 60 °C is 0.7% and 2.1%, respectively.

The nature of interface/interfacial adhesion is a crucial factor that determines the stress transfer between the reinforcing fibers and the matrix and thereby the mechanical properties of the corresponding composites. The IFSS is the parameter that signifies the interfacial property of the composites and their values for AF/epoxy composites prepared at different treatment conditions are presented in Table 3. Evidently, the IFSS of the modified aramid/epoxy composites was significantly higher than that of the unmodified aramid/epoxy composites. The IFSS of AF/epoxy composites was significantly improved with the modification in AF surface due to the increased surface roughness of AF with the treatment of dopamine and amino GO. This is mainly because that the increase of AF surface roughness can improve the surface activity of fibers and the interaction with resins. It is important to note that the IFSS of composites comprising amino GO/PDA-AF is slightly lower than that of the composites comprising the PDA-AFs at a lower reaction temperature of 40 °C. Although the roughness of the fiber surface increased relatively, the bonding strength between dopamine and aramid fiber was not too high, and the interface between dopamine and aramid fiber was preferred to be separated from the composite material when it was pulled away. Interestingly, the IFSS of composites comprising amino GO/PDA-AF was higher than that of the composites comprising PDA-AFs at a higher reaction temperature of 60 °C. The amino GO improved the polarity and surface reactivity of PDA-AF by introducing the reactive functional groups, thereby improving the wettability and interfacial properties of AF/epoxy interface [39]. Moreover, the inherent high specific surface area of amino GO contributed to the IFSS by consuming the destructive energy [23].

4. Conclusions

Aramid fibers were modified by self-oxidative polymerization of dopamine and amino GO grafting. XPS and SEM results confirmed that aramid fibers were coated with PDA and amino GO. The amino GO grafting improved the surface roughness, polarity and reactivity of the PDA-AF. The amount of amino GO grafting was altered by changing the reaction temperature and concentration of ethylenediamine. At a higher reaction temperature of 60 °C, amino GO/PDA-AF/epoxy composites exhibited IFSS of 35.21 MPa, which was 34% higher than that of pure-AF/epoxy composites (26.31 MPa). The improved IFSS demonstrated the satisfactory reinforcing was achieved by modification of aramid fibers. This study delivers the facile route for the surface modification of high-performance fibers for their potential applications in multifunctional polymer composites especially with functional nanoparticles [40–49] and functional polymers [50–55] for various applications such as electromagnetic interface shielding [56–59], environmental remediation [60–64] and sensing [65–69].

Acknowledgments

The authors gratefully acknowledge the financial support by the National Natural Science Foundation of China (NSFC grant no. 51790502), the Harbin University Doctor Foundation by no. HUDF2017101 and Key Laboratory of Functional Inorganic Material Chemistry (Heilongjiang University), Ministry of Education, China.

References

[1] J.M. García, F.C. García, F. Serna, J.L. de la Peña, High-performance aromatic polyamides, Prog. Polym. Sci. 35 (5) (2010) 623–686.
[2] G. Tang, Z.-G. Jiang, X. Li, H.-B. Zhang, S. Hong, Z.-Z. Yu, Electrically conductive rubbery epoxy/diamine-functionalized graphene nanocomposites with improved mechanical properties, Compos., Part B 67 (2014) 564–570.
[3] J. Zhao, Effect of surface treatment on the structure and properties of para-aramid fibers by phosphoric acid, Fibers Polym. 14 (1) (2013) 59–64.
[4] M. Mukherjee, C.K. Das, A.P. Kharitonov, et al., Properties of syndiotactic polystyrene composites with surface modified short Kevlar fiber, Mater. Sci. Eng., A 441

(1) (2006) 206–214.
[5] J. Gao, Y. Dai, X. Wang, et al., Effects of different fluorination routes on aramid fiber surface structures and interlaminar shear strength of its composites, Appl. Surf. Sci. 270 (2013) 627–633.
[6] C. Wang, V. Murugadoss, J. Kong, et al., Overview of carbon nanostructures and nanocomposites for electromagnetic wave shielding, Carbon 140 (2018) 696–733.
[7] Z. Wang, R. Wei, J. Gu, et al., Ultralight, highly compressible and fire-retardant graphene aerogel with self-adjustable electromagnetic wave absorption, Carbon 139 (2018) 1126–1135.
[8] M.S. Islam, Y. Deng, L. Tong, S.N. Faisal, A.K. Roy, A.I. Minett, V.G. Gomes, Grafting carbon nanotubes directly onto carbon fibers for superior mechanical stability: towards next generation aerospace composites and energy storage applications, Carbon 96 (2016) 701–710.
[9] A. Vaish, S.G. Roy, P. De, Synthesis of amino acid based covalently cross-linked polymeric gels using tetrakis(hydroxymethyl) phosphonium chloride as a cross-linker, Polymer 58 (2015) 1–8.
[10] R. Gu, J. Yu, C. Hu, L. Chen, J. Zhu, Z. Hu, Surface treatment of para-aramid fiber by argon dielectric barrier discharge plasma at atmospheric pressure, Appl. Surf. Sci. 258 (2012) 10168–10174.
[11] S. Li, K. Han, H. Rong, X. Li, M. Yu, Surface modification of aramid fibers via ammonia-plasma treatment, J. Appl. Polym. Sci. 131 (10) (2013).
[12] Z. Wu, H. Cui, L. Chen, et al., Interfacially reinforced unsaturated polyester carbon fiber composites with a vinyl ester-carbon nanotubes sizing agent, Compos. Sci. Technol. 164 (2018) 195–203.
[13] Z. Wu, S. Gao, L. Chen, et al., Electrically insulated epoxy nanocomposites reinforced with synergistic core-shell SiO_2@MWCNTs and montmorillonite bifillers, Macromol. Chem. Phys. 218 (2017) 1700357.
[14] Y.M. Shin, Y.B. Lee, S.J. Kim, J.K. Kang, J.-C. Park, W. Jang, H. Shin, Mussel-inspired immobilization of vascular endothelial growth factor (VEGF) for enhanced endothelialization of vascular grafts, Biomacromolecules 13 (7) (2012) 2020–2028.
[15] W. Wang, R. Li, M. Tian, et al., Surface silverized meta-aramid fibers prepared by bio-inspired poly(dopamine) functionalization, ACS Appl. Mater. Interfaces 5 (6) (2013) 2062–2069.
[16] L. Yang, S.L. Phua, C.L. Toh, et al., Polydopamine-coated graphene as multifunctional nanofillers in polyurethane, RSC Adv. 3 (18) (2013) 6377–6385.
[17] W.J. Yang, K.-G. Neoh, E.-T. Kang, S. Lay-Ming Teo, D. Rittschof, Stainless steel surfaces with thiol-terminated hyperbranched polymers for functionalization via thiol-based chemistry, Polym. Chem. 4 (10) (2013) 3105–3115.
[18] S.L. Phua, L. Yang, C.L. Toh, et al., Reinforcement of polyether polyurethane with dopamine-modified clay: the role of interfacial hydrogen bonding, ACS Appl. Mater. Interfaces 4 (9) (2012) 4571–4578.
[19] S. Chen, Y. Cao, J. Feng, Polydopamine as an efficient and robust platform to functionalize carbon fiber for high-performance polymer composites, ACS Appl. Mater. Interfaces 6 (1) (2014) 349–356.
[20] J. Zhu, L. Yuan, Q. Guan, G. Liang, A. Gu, A novel strategy of fabricating high performance UV-resistant aramid fibers with simultaneously improved surface activity, thermal and mechanical properties through building polydopamine and graphene oxide bi-layer coatings, Chem. Eng. J. 310 (2017) 134–147.
[21] R. Sa, Y. Yan, Z. Wei, L. Zhang, W. Wang, M. Tian, Surface modification of aramid fibers by bio-inspired poly(dopamine) and epoxy functionalized silane grafting, ACS Appl. Mater. Interfaces 6 (23) (2014) 21730–21738.
[22] L. Zhao, H. Zhang, N.H. Kim, D. Hui, J.H. Lee, Q. Li, H. Sun, P. Li, Preparation of graphene oxide/polyethyleneimine layer-by-layer assembled film for enhanced hydrogen barrier property, Composites, Part B 92 (2016) 252–258.
[23] C. Wang, M. Zhao, J. Li, et al., Silver nanoparticles/graphene oxide decorated carbon fiber synergistic reinforcement in epoxy-based composites, Polymer 131 (2017) 263–271.
[24] S. Wang, Z.-H. Chen, W.-J. Ma, Q.-S. Ma, Influence of heat treatment on physical–chemical properties of PAN-based carbon fiber, Ceram. Int. 32 (3) (2006) 291–295.
[25] W. Wang, Y. Jiang, Y. Liao, et al., Fabrication of silver-coated silica microspheres through mussel-inspired surface functionalization, J. Colloid Interface Sci. 358 (2) (2011) 567–574.
[26] Y. Long, J. Wu, H. Wang, X. Zhang, N. Zhao, J. Xu, Rapid sintering of silver nanoparticles in an electrolyte solution at room temperature and its application to fabricate conductive silver films using polydopamine as adhesive layers, J. Mater. Chem. 21 (13) (2011) 4875–4881.
[27] C.M. Preuss, A.S. Goldmann, V. Trouillet, A. Walther, C. Barner-Kowollik, Biomimetic dopamine-diels–alder switches, Macromol. Rapid Commun. 34 (8) (2013) 640–644.
[28] Z. Yang, X. Hao, S. Chen, et al., Long-term antibacterial stable reduced graphene oxide nanocomposites loaded with cuprous oxide nanoparticles, J. Colloid Interface Sci. 533 (2019) 13–23.
[29] V. Murugadoss, N. Wang, S. Tadakamalla, B. Wang, Z. Guo, S. Angaiah, In situ grown cobalt selenide/graphene nanocomposite counter electrodes for enhanced dye-sensitized solar cell performance, J. Mater. Chem. 5 (2017) 14583–14594.
[30] Y. He, S. Yang, H. Liu, et al., Reinforced carbon fiber laminates with oriented carbon nanotube epoxy nanocomposites: magnetic field assisted alignment and cryogenic temperature mechanical properties, J. Colloid Interface Sci. 517 (2018) 40–51.
[31] I. Zaman, T.T. Phan, H.C. Kuan, et al., Epoxy/graphene platelets nanocomposites with two levels of interface strength, Polymer 52 (7) (2011) 1603–1611.
[32] B. Kirubasankar, V. Murugadoss, J. Lin, et al., In situ grown nickel selenide on graphene nanohybrid electrodes for high energy density asymmetric supercapacitors, Nanoscale 10 (43) (2018) 20414–20425.
[33] M.S. Dresselhaus, A. Jorio, L.G. Cançado, G. Dresselhaus, R. Saito, Raman spectroscopy: characterization of edges, defects, and the fermi energy of graphene and sp2 carbons, in: H. Raza (Ed.), Graphene Nanoelectronics: Metrology, Synthesis, Properties and Applications, Springer Berlin Heidelberg, Berlin, Heidelberg, 2012, pp. 15–55.
[34] L. Zhu, Y. Lu, Y. Wang, L. Zhang, W. Wang, Preparation and characterization of dopamine-decorated hydrophilic carbon black, Appl. Surf. Sci. 258 (14) (2012) 5387–5393.
[35] W. Cui, M. Li, J. Liu, B. Wang, C. Zhang, L. Jiang, Q. Cheng, A strong integrated strength and toughness artificial nacre based on dopamine cross-linked graphene oxide, ACS Nano 8 (9) (2014) 9511–9517.
[36] X. Li, G.B. McKenna, G. Miquelard-Garnier, A. Guinault, C. Sollogoub, G. Regnier, A. Rozanski, Forced assembly by multilayer coextrusion to create oriented graphene reinforced polymer nanocomposites, Polymer 55 (1) (2014) 248–257.
[37] J. Zhang, H. Yang, G. Shen, P. Cheng, J. Zhang, S. Guo, Reduction of graphene oxide vial-ascorbic acid, Chem. Commun. 46 (7) (2010) 1112–1114.
[38] X.J. Shen, L.X. Meng, Z.Y. Yan, et al., Improved cryogenic interlaminar shear strength of glass fabric/epoxy composites by graphene oxide, Compos. B 73 (2015) 126–131.
[39] J. Chen, D. Zhao, X. Jin, C. Wang, D. Wang, H. Ge, Modifying glass fibers with graphene oxide: towards high-performance polymer composites, Compos. Sci. Technol. 97 (2014) 41–45.
[40] Y. Jiao, J. Zhang, S. Liu, Y. Liang, S. Li, H. Zhou, J. Zhang, The graphene oxide ionic solvent-free nanofluids and their battery performances, Sci. Adv. Mater. 10 (2018) 1706–1713.
[41] Z. Zhao, P. Bai, L. Li, J. Li, L. Wu, P. Huo, L. Tan, The reaction thermodynamics during plating Al on graphene process, Materials 12 (2) (2019) 330.
[42] Y. Zhao, X. Tian, et al., Precipitation sequence of middle Al concentration alloy using the inversion algorithm and microscopic phase field model, Sci. Adv. Mater. 10 (2018) 1793–1804.
[43] Y. Sheng, J. Yang, F. Wang, et al., Sol-gel synthesized hexagonal boron nitride/titania nanocomposites with enhanced photocatalytic activity, Appl. Surf. Sci. 465 (2019) 154–163.
[44] M. Dong, Q. Li, H. Liu, C. Liu, E. Wujcik, Q. Shao, T. Ding, X. Mai, C. Shen, Z. Guo, Thermoplastic polyurethane-carbon black nanocomposite coating: fabrication and solid particle erosion resistance, Polymer 158 (2018) 381–390.
[45] W. Du, X. Wang, J. Zhan, X. Sun, et al., Biological cell template synthesis of nitrogen-doped porous hollow carbon spheres/MnO_2 composites for high-performance asymmetric supercapacitors, Electrochim. Acta 296 (2019) 907–915.
[46] J. Zhang, P. Li, Z. Zhang, X. Wang, J. Tang, H. Liu, Q. Shao, T. Ding, A. Umar, Z. Guo, Solvent-free graphene liquids: promising candidates for lubricants without the base oil, J. Colloid Interface Sci. 542 (2019) 159–167, https://doi.org/10.1016/j.jcis.2019.01.135 in press.
[47] R. Li, X. Zhu, Q. Fu, et al., Nanosheet-based $Nb_{12}O_{29}$ hierarchical microspheres for enhanced lithium storage, Chem. Commun. (2019), https://doi.org/10.1039/C8CC09924C in press.
[48] Y. Li, T. Jing, G. Xu, J. Tian, et al., 3-D magnetic graphene oxide-magnetite poly (vinyl alcohol) nanocomposite substrates for immobilizing enzyme, Polymer 149 (2018) 13–22.
[49] X. Cui, G. Zhu, Y. Pan, Q. Shao, et al., Polydimethylsiloxane-titania nanocomposite coating: fabrication and corrosion resistance, Polymer 138 (2018) 203–210.
[50] C. Wang, Z. He, X. Xie, X. Mai, et al., Controllable cross-linking anion exchange membranes with excellent mechanical and thermal properties, Macromol. Mater. Eng. 3 (2018) 1700462.
[51] Y. Zhang, M. Zhao, J. Zhang, et al., Excellent corrosion protection performance of epoxy composite coatings filled with silane functionalized silicon nitride, J. Polym. Res. 25 (2018) 130.
[52] C. Wang, B. Mo, Z. He, et al., Crosslinked norbornene copolymer anion exchange membrane for fuel cells, J. Membr. Sci. 556 (2018) 118–125.
[53] Z. Hu, D. Zhang, F. Lu, W. Yuan, et al., Multistimuli-responsive intrinsic self-healing epoxy resin constructed by host – guest interactions, Macromolecules 51 (2018) 5294–5303.
[54] Z. Hu, Y. Liu, X. Xu, et al., Efficient intrinsic self-healing epoxy acrylate formed from host-guest chemistry, Polymer 164 (2019) 79–85.
[55] C. Wang, B. Mo, Z. He, et al., Hydroxide ions transportation in polynorbornene anion exchange membrane, Polymer 138 (2018) 363–368.
[56] D. Jiang, V. Murugadoss, Y. Wang, et al., Electromagnetic interference shielding polymers and nanocomposites – a review, Polym. Rev. (2018), https://doi.org/10.1080/15583724.2018.1546737 in press.
[57] N. Wu, C. Liu, D. Xu, et al., Ultrathin high-performance electromagnetic wave absorbers with facilely fabricated hierarchical porous Co/C crabapples, J. Mater. Chem. C 7 (2019) 1659–1669, https://doi.org/10.1039/C8TC04984J in press.
[58] N. Wu, D. Xu, Z. Wang, et al., Achieving superior electromagnetic wave absorbers through the novel metal-organic frameworks derived magnetic porous carbon nanorods, Carbon 145 (2019) 433–444.
[59] N. Wu, C. Liu, D. Xu, et al., Enhanced electromagnetic wave absorption of three-dimensional porous Fe3O4/C composite flowers, ACS Sustain. Chem. Eng. 6 (2018) 12471–12480.
[60] Z. Li, B. Wang, X. Qin, et al., Superhydrophobic/superoleophilic polycarbonate/carbon nanotubes porous monolith for selective oil adsorption from water, ACS Sustain. Chem. Eng. 6 (2018) 13747–13755.
[61] Y. Ma, L. Lyu, Y. Guo, et al., Porous lignin based poly (acrylic acid)/organo-montmorillonite nanocomposites: swelling behaviors and rapid removal of Pb (II) ions, Polymer 128 (2017) 12–23.
[62] K. Gong, Q. Hu, L. Yao, et al., Ultrasonic pretreated sludge derived stable magnetic active carbon for Cr(VI) removal from wastewater, ACS Sustain. Chem. Eng. 6 (2018) 7283–7291.
[63] H. Zhang, S. Lyu, X. Zhou, et al., Super light 3D hierarchical nanocellulose aerogel

foam with superior oil adsorption, J. Colloid Interface Sci. 536 (2019) 245–251.
[64] Y. Qian, Y. Yuan, H. Wang, et al., Highly efficient uranium adsorption by salicylaldoxime/polydopamine graphene oxide nanocomposites, J. Mater. Chem. A 6 (2018) 24676–24685.
[65] H. Gu, H. Zhang, J. Lin, et al., Large negative giant magnetoresistance at room temperature and electrical transport in cobalt ferrite-polyaniline nanocomposites, Polymer 143 (2018) 324–330.
[66] H. Liu, Q. Li, S. Zhang, et al., Electrically conductive polymer composites for smart flexible strain sensor: a critical review, J. Mater. Chem. C 6 (2018) 12121–12141.
[67] H. Gu, H. Zhang, C. Ma, et al., Smart strain sensing organic-inorganic hybrid hydrogels with nano barrium ferrite as cross-linker, J. Mater. Chem. C (2019), https://doi.org/10.1039/C8TC05448G in press.
[68] H. Wei, H. Wang, Y. Xia, et al., An overview of lead-free piezoelectric materials and devices, J. Mater. Chem. C 6 (2018) 12446–12467.
[69] Y. Lu, M.C. Biswas, Z. Guo, J. Jeon, E.K. Wujcik, Recent developments in bio-monitoring via advanced polymer nanocomposite-based wearable strain sensors, Biosens. Bioelectron. 123 (2019) 167–177.